JGR Solid Earth

RESEARCH ARTICLE
10.1029/2023JB027332

Special Section:
Heterogeneity, anisotropy and scale-dependency: Keys to understand Earth composition, structure and behavior

Heterogeneity-Driven Localization and Weakening in Scaly Clays From a Fossil Accretionary Prism

S. Aretusini[1], S. Mittempergher[2], F. Remitti[2], R. Arletti[2], M. Polisi[2], N. De Paola[3], and T. Tesei[4]

[1]Istituto Nazionale di Geofisica e Vulcanologia, Roma, Italy, [2]Università di Modena e Reggio Emilia, Modena, Italy, [3]University of Durham, Durham, UK, [4]Università degli Studi di Padova, Padova, Italy

Key Points:

- Experimental deformation of natural scaly clays at 10–120 MPa and 25–150°C
- Strain localization and weakening occur when a pre-existing lithological contact is included in the sample and at high P-T conditions
- Lithological contacts and water release enhance strain localization and weakening in natural accretionary prisms

Supporting Information:

Supporting Information may be found in the online version of this article.

Correspondence to:

S. Aretusini,
stefano.aretusini@ingv.it

Citation:

Aretusini, S., Mittempergher, S., Remitti, F., Arletti, R., Polisi, M., De Paola, N., & Tesei, T. (2023). Heterogeneity-driven localization and weakening in scaly clays from a fossil accretionary prism. *Journal of Geophysical Research: Solid Earth*, *128*, e2023JB027332. https://doi.org/10.1029/2023JB027332

Received 29 JUN 2023
Accepted 14 AUG 2023

Author Contributions:

Conceptualization: S. Aretusini, S. Mittempergher, F. Remitti, T. Tesei
Data curation: S. Aretusini
Formal analysis: S. Aretusini, T. Tesei
Funding acquisition: T. Tesei
Investigation: R. Arletti, M. Polisi, T. Tesei

Abstract In accretionary prisms, scaly clays structure might be the result of strain localization and weakening or strain delocalization and hardening. Therefore, it is not clear how they influence the mechanical behavior of the accretionary prism. Here, we investigate the effect of rock fabric on the mechanical properties of scaly clays sampled from a fossil accretionary prism in a range of pressure-temperature conditions typical of burial within accretionary prisms. We performed triaxial experiments using a direct shear configuration on samples in which the natural scaly clay fabric and natural lithological boundaries were preserved, at confining pressures of 10–120 MPa and temperatures of 25–150°C. Samples with homogeneous composition and natural scaly fabrics display strain hardening behavior at all tested conditions. Shearing at high P-T displays lower strength with respect to shearing at low P-T. The samples containing a lithological contact display strain hardening at low P-T and weakening at high P-T conditions. After the experiments, the homogeneous samples show a distributed foliation and short, discontinuous shear surfaces at the contacts with the sample holder, while the samples including a contact developed a through-going shear zone composed of a series of en-echelon shear surfaces. A reduced smectite and water content is observed in the post-deformation samples, suggesting that weakening may correlate with water release during dehydration reactions of clay minerals at 150°C. This shows how both dehydration reactions at high P-T conditions and strain localization along lithological boundaries promote brittle behavior within scaly clays in subduction zones accretionary prisms.

Plain Language Summary In subduction zones, among the rocks that constitute the accretionary prism are claystones with a peculiar texture called "scaly clays." We investigated these rocks preserving their original scaly texture at deformation and temperature conditions typical of those occurring in the frontal part of subduction zone. In the deformed samples, only when a contact between two different scaly clays is present and it is deformed at the highest pressure and temperature, a decrease of strength occurs. This behavior is related to the simultaneous presence of a pre-existing lithological contact across the sample and by the release of water by dehydration of the "scaly clays." The process, reproduced in the laboratory, might occur at a larger scale and control deformation within the natural subduction zones.

1. Introduction

The rheology of rocks and sediments in the accretionary prisms of subduction zones influence the mechanics of megathrusts at the plate boundary interface. Among the accretionary prism rocks, pelagic sediments enriched in smectite clay minerals were widely studied to interpret the mechanics of shallow subduction zones (Byrne & Fisher, 1990; Oleskevich et al., 1999; Vrolijk, 1990). In particular, for the Pacific Plate subduction zones, pelagic clays can be an important component of the plate boundary fault and therefore influence the size of shallow subduction zone earthquakes (Hilde, 1983; J. C. Moore et al., 2015; Sawai et al., 2014). Early studies (e.g., J. C. Moore & Saffer, 2001; Vrolijk, 1990) suggested that a key role is played by low grade reactions, such as the decomposition of smectite into illite (Vrolijk, 1990). However, recent studies highlight that shallow depth seismicity is controlled by many structural and material property factors (Saffer & Tobin, 2011). In particular, strain localization mechanisms within clay-rich subducted rocks are affected by fabric development, lithological contrasts and by the release of pressurized fluids due to porosity reduction by sediment compaction or to dehydration of minerals (Byrne & Fisher, 1990; Kubo & Katayama, 2015; D. E. Moore & Lockner, 2007; Vannucchi et al., 2008; Tesei et al., 2015).

Methodology: S. Aretusini, R. Arletti, M. Polisi
Resources: S. Mittempergher, F. Remitti, R. Arletti, M. Polisi, N. De Paola
Supervision: T. Tesei
Validation: R. Arletti, T. Tesei
Visualization: S. Aretusini
Writing – original draft: S. Aretusini
Writing – review & editing: S. Aretusini, S. Mittempergher, F. Remitti, R. Arletti, N. De Paola, T. Tesei

Pelagic clays in accretionary prisms can display a distinctive "scaly fabric" consisting of anastomosing slip surfaces wrapped around mm-to-cm-sized lozenge-shaped lithons, with their major axis parallel to the S-foliation direction. Scaly fabric commonly forms in response to shearing along a fault zone (Kirkpatrick et al., 2015; Maltman & Vannucchi, 2004; J. C. Moore, 1986; Schleicher et al., 2010; Vannucchi et al., 2003) or for flexural slip in fold limbs (Bettelli & Vannucchi, 2003; Vannucchi et al., 2003). The scaly clay domains can reach a thickness of several m to 100s of m, and bulk deformation is accompanied by sharp and localized shear surfaces (Cowan & Silling, 1978; Festa et al., 2009; Kirkpatrick et al., 2015; Labaume et al., 1997; Pini, 1999; Vannucchi, 2019; Vannucchi et al., 2003).

The rheology of scaly clays is difficult to investigate due to the intrinsic difficulties in sample preparation, which normally results in studying remolded samples, therefore losing the original fabric. Nevertheless, previous studies show that rock fabrics exerts a strong control on frictional strength, stability and healing of faults, promoting a broad spectrum of slip behaviors (Collettini et al., 2009; Ikari et al., 2015; Tesei et al., 2014). Overall, is poorly known how the localization versus de-localization of strain in scaly clays is associated to the progressive effect of water release, first by compaction an then by low-grade metamorphic reactions. However, improving the knowledge of the localization processes might shed light on the hardening and weakening processes and on the ductile versus brittle failure behavior that influence the occurrence of aseismic or seismic deformation in these rocks.

Here, for the first time, we document the mechanical behavior of natural scaly fabrics sheared intact in a triaxial apparatus at temperatures (20 and 150°C) and confining pressures (10–120 MPa), typical of those conditions achieved during progressive burial beneath an accretionary prism. Scaly clays used during the experiments were retrieved from an exhumed accretionary prism in the Northern Apennines (Bettelli & Vannucchi, 2003; Remitti et al., 2012, 2013). We sampled across a lithological boundary which underwent shear during flexural slip (hereon "lithological contact") between two strata of pelagic claystones. We show that, at the highest experimental P-T conditions, the presence of the lithological contact is a necessary condition to drive weakening and strain localization.

2. Geological Setting

The External Ligurian Units are non-metamorphic units that are composed of a clay-rich sequence ("basal Units," Remitti et al., 2012) and an overlying thick pile of calcareous and/or siliciclastic turbidites (i.e., the Late Cretaceous Helminthoid flysches and the External Ligurian flysch of early to middle Eocene age). The deformation style of both units has been interpreted as the result of offscraping and frontal accretion during the closure of the branch of the Tethys Ocean interposed between the Europa and Adria plates (Bettelli & Vannucchi, 2003; Vannucchi & Bettelli, 2002).

The lack of metamorphic overprint implies that stratal disruption occurred at shallow depth, consistent with the interpretation that the Ligurian multilayers were assembled by frontal accretion (Vannucchi & Bettelli, 2002). This setting is constrained by the presence of the slope apron sequence, the Epiligurian Succession, resting on an unconformity on top of the Ligurian Units. A regional thermochronological study suggested that the Ligurian Units experienced maximum temperatures of less than 70°C, compatible with the burial due to the overlying Epiligurian Units (Thomson et al., 2010).

The basal Units typically crop out as broken formations, showing a complex deformation pattern with at least two generations of superimposed mesoscopic folds (see Figure 4 in Bettelli & Vannucchi, 2003). The older folds, F1, are usually of metric scale, close to isoclinal, and highly non-cylindrical, locally even sheath folds. The second generation of folds, F2, has the same characteristics as F1, except for their disharmonic style developed as a consequence of the interference with F1 folds. A third folding event, F3, is locally observable with open, recumbent, northeast-vergent folds. F2 and F3 are coaxial, and the latter may be a further evolution of F2, rather than a discrete new folding phase. The rocks folded by F1 and F2 show a continuous and progressive increase in diagenetic conditions through the different deformation stages. This evolution has been interpreted as continuous deformation and burial within an accretionary prism and not as different tectonic phases during the Apennines orogeny (Vannucchi & Bettelli, 2002).

The samples used in this study consist of shales of the "Argille Varicolori" (AVV) (Bettelli & Vannucchi, 2003). They are formed of thin-bedded shales with sparse beds of turbidite limestones, sandstones, marlstones, and limestones (Figure 1), are of Late Cretaceous age, and are interpreted as abyssal plain deposits. In rare low-strain

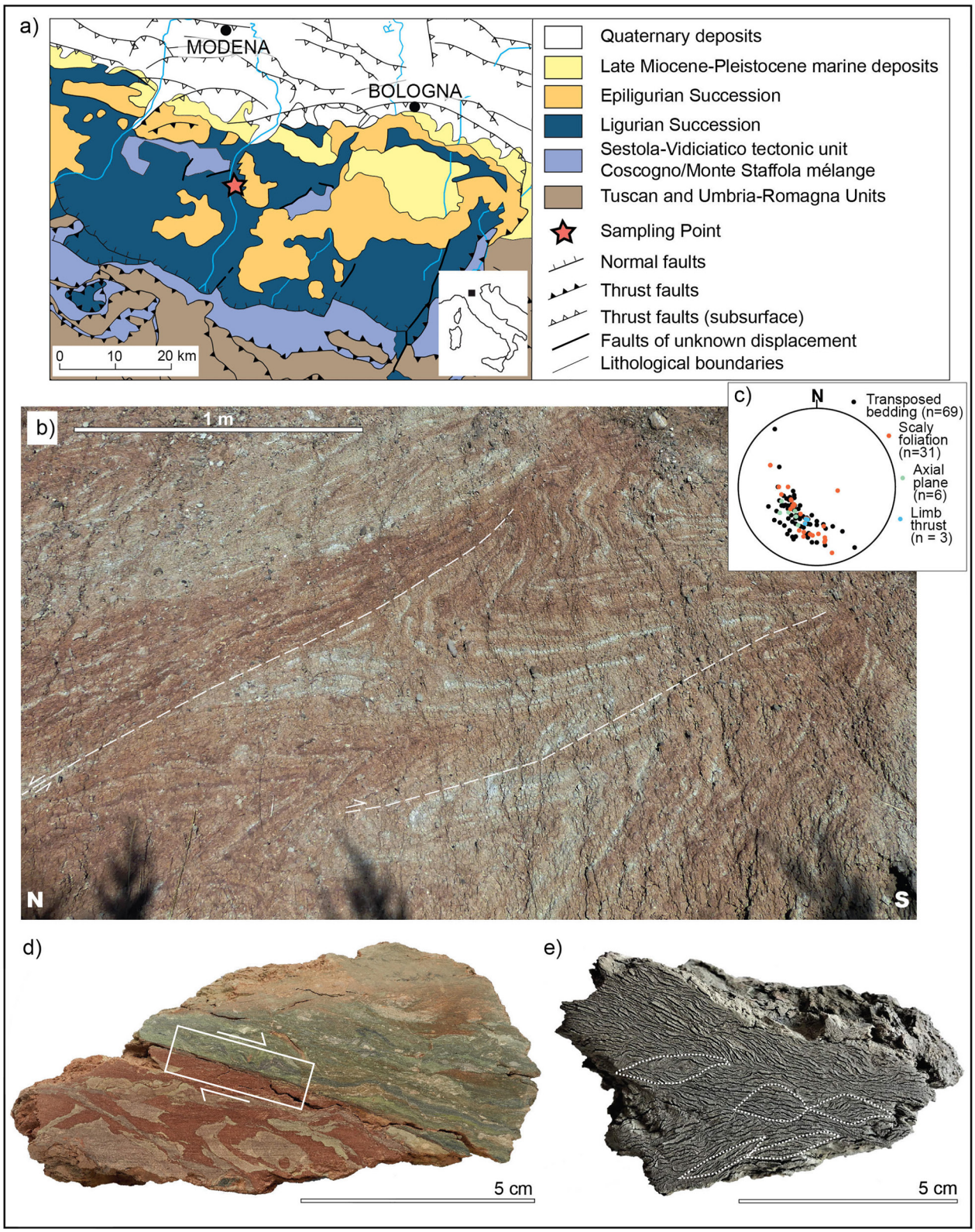

Figure 1.

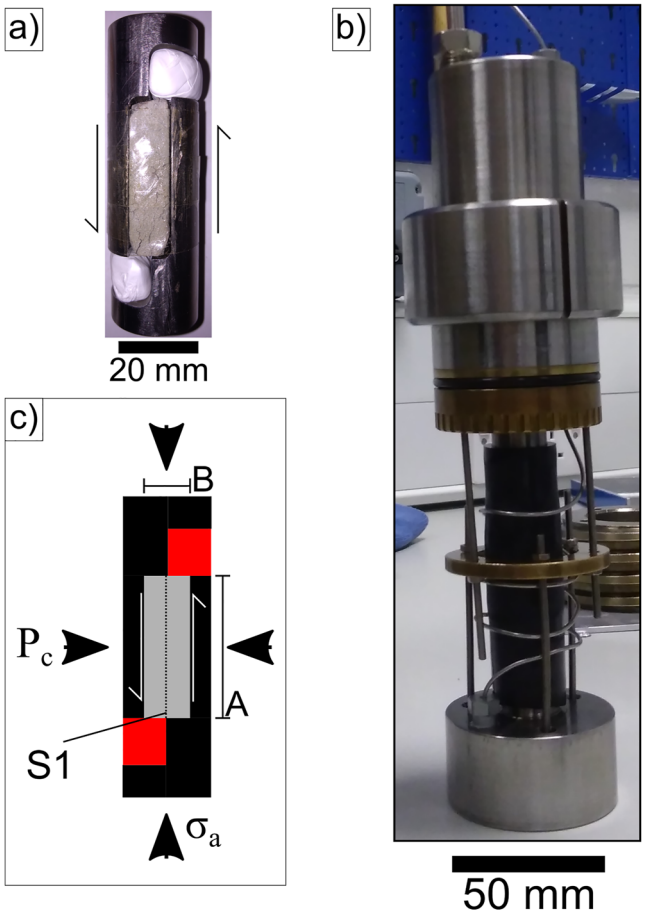

Figure 2. Sample assemblage. (a) Photo of the sample before inserting it in the assembly, (b) photo of the sample assembly before insertion in the pressure vessel, (c) sketch showing the orientation of confinement pressure P_c, and axial stress σ_a with respect to the sample (gray), and cross sectional areas A and B. L-shaped pistons (black) and rubber spacers (red) are also shown.

domains, the AVV preserve their sedimentary organisation consisting of intercalated thin to medium (1–10 cm) shaly layers of different colors (red, green, black, light gray, whitish). Elsewhere, the original beds appear as stretched, discontinuous and irregular bands parallel to a pervasive scaly fabric (Vannucchi & Bettelli, 2002), defining a transposed foliation S1. Along with folding, the AVVs display other deformation structures including boudinage of competent layers, limb thrusts, mud injections, swirls, limb thinning and hinge thickening. Despite significant shearing having occurred along the original bed interfaces during foliation transposition and, at a larger scale, along limb thrusts, the boundaries between clays of different colors remain generally very sharp (Figure 1d).

3. Methods

3.1. Field Sampling

We sampled clay blocks in an outcrop within a quarry excavated in the Argille Varicolori multilayer rocks (Figure 1, coordinates: 44°21′43.2″N 10°56′13.2″E). The outcrop included a well recognizable sheared lithological boundary that puts in contact red and gray pelagic clays. This boundary is now an isoclinal fold limb (parallel to the transposed foliation S1 discussed above), with evidence of stretching and boudinage parallel to the fold limbs. The lithological boundary is roughly parallel to orientation of the main shear planes defining the lithons of the scaly clays (Figure 1c). We retrieved samples for lab experiments from three starting materials: (a) gray clay, (b) red clay, and (c) the red-on-gray clay with the lithological contact in between.

3.2. Sample Preparation and Triaxial Direct Shear Experiments

The original samples were reduced in size with a diamond wheel saw and then shaped into blocks (40 × 20 × 8 or 30 × 20 × 8 mm) using wet sandpaper, to fit the experimental sample holders (Figure S1 in Supporting Information S1). While doing so, the base of each block was oriented parallel to the lithological contact surface or the macroscopic S1-foliation direction of the scaly fabric. Afterward, samples were air-dried at room temperature overnight to remove excess moisture. Ovens were not used to avoid shrinkage cracking of the samples, and to keep adsorbed water for experimental testing at undrained conditions (see below).

A total of nine experiments were done on the block samples under direct shear configuration into a triaxial apparatus hosted at Durham University (Harbord et al., 2017). All experimental conditions are provided in Table S1 in Supporting Information S1. The blocks were sandwiched between two L-shaped forcing pistons with rubber and Teflon spacers, jacketed, and the resulting assembly was placed into a pressure vessel (Figures 2a and 2b). The confining pressure P_c applied by the triaxial apparatus was equivalent to the normal stress σ_n on the base surface of our samples (i.e., the surface parallel to the shear sense, "A" in Figure 2c). During the whole experiment, samples were kept undrained so that no exchange of pore fluid from the sample to the pore fluid pressure lines was possible. The vertical piston was advanced (from bottom to top of the pressure vessel) with controlled axial rate of 1 μm/s and was used to apply a force parallel to the axis of the cylindrical sample assembly. The axial force was measured with an internal load cell. The experimental protocol consisted of two phases, a low and high P-T

Figure 1. Geological setting. (a) Geologic map of part of the Northern Apennines area, modified from (Bettelli & De Nardo, 2001; Vannucchi et al., 2008), with the location of the sampling site highlighted by a red star. (b) Field photo of an outcrop near the sampling site with the rocks from the accretionary prism forming nearly isoclinal folds with stretching and shearing parallel to the fold limbs (white dashed lines). (c) Stereoplot of the poles of transposed bedding, scaly fabric flattening planes, axial planes and sheared limbs planes, lower hemisphere equiangular projection. (d) Polished hand sample including the sharp and localized contact of red-on-gray clay. The white box (30 × 10 mm) represents the size our experimental samples and the shear sense during the experiments, coherent with the inferred shear sense of the natural lithological contact is indicated. (e) Hand sample of a gray clay sample wetted with water and shrunk to highlight the pervasive foliation of the scaly clay fabric. Five scaly clays are highlighted by a white dashed line.

stage respectively. During the low P-T stage of the experiment, the sample assembly was loaded in the pressure vessel, and while keeping the confinement oil at room temperature (ca. 22°C), we applied the confining pressure of 10, 30, or 50 MPa. Then, after we achieved touchpoint (i.e., closed the axial gap between the vertical piston and the base of the assembly), we advanced the vertical piston at a rate of 1 μm/s for 1.8–2.3 mm. After shearing the sample at constant velocity, we imposed a sequence of slide-hold-slide steps, consisting of sliding at 1 μm/s for 0.2–0.25 mm interspersed with hold times of 10, 30, 100, 300, 1,000, 3,000 s. After the low P-T stage of the experiment, we started the high P-T stage by lowering the axial piston until it was detached from the base of the sample assembly. Then, the confinement oil in the pressure vessel was heated up to 150°C in 2 hr, the heating rate was controlled by the internal thermocouple in contact with the sample. The sample was allowed to equilibrate to the target temperature for another minimum 2 hr. After the equilibration time, we applied the confining pressure of 80, 100, or 120 MPa, and loaded the sample by repeating the same constant velocity shearing and slide-hold-slide sequence as above. Before each touchpoint, the axial force was zeroed and divided by the basal contact area of the sample (20 mm × 8 mm, "B" in Figure 2c) to obtain the axial stress σ_a.

After the experiments, the samples were air dried at room humidity and temperature and then embedded into Struers Epofix® epoxy resin. Then, they were dry cut with a diamond wheel saw in the direction parallel to the longer side of the sample block to obtain three slices per sample. One side of the sliced sample was then dry polished and scanned to obtain a cross section image of the sheared sample. On the cross section we measured the apparent offset developed with the shear deformation (see Table S1 in Supporting Information S1). From red-on-gray d321, gray d318, and red d332 samples cross section we obtained Back Scattered Electron images using a JEOL JSM-6500F Field Emission Scanning Electron Microscope host at INGV, Rome, setup with 15 kV electron column voltage and ca. 10 mm working distance. Due to the low contrast between the mineral phases composing the samples, back-scattered images were enhanced using an adaptive histogram equalization algorithm available in Matlab®.

3.3. Analyses on the Starting and Deformed Samples

X-ray powder diffraction (XRPD) measurements, thermogravimetric (TG), and differential thermal analysis (DTA) measurements were performed both on undeformed samples and on the 1/3 slice obtained from the samples deformed after the experiments. Gray clays deformed in experiment d336, and red clays in experiment d334 were chosen as they were deformed at the highest confining pressure.

Before the XRPD analysis, the samples were air dried and the entire layer thickness recovered to avoid partial sampling. The gouge layer was gently disaggregated with a pestle and mortar. The resulting powders were: (a) mounted laterally on an aluminum sample holder to avoid isorientation of the clay minerals upon sample preparation; (b) isoriented using the glass slide method, and (c) isoriented with the glass slide method and glycolated. Data was collected with a θ/θ diffractometer PANalytical X'Pert Pro (University of Modena and Reggio Emilia, Modena, Italy) equipped with a real time multiple strip detector (X'Celerator), using CuKα radiation ($K\alpha_1$: 1.54059 Å and $K\alpha_2$: 1.54440 Å) and 1°/2° divergent and antiscatter slits. For the determination of mineral phases, diffraction data was acquired in the 4°–90°2θ range, with a step size of 0.017°2θ and scan step time of 102 s. For the identification of clay mineral phases, diffraction data was acquired in the 3°–14°2θ range, using the same scanning conditions.

TG and DTA analysis were performed with a Seiko SSC/5200 (University of Modena and Reggio Emilia, Modena, Italy). Each sample weighed 20 mg and was positioned into a Pt crucible. The thermal analyses were performed in the range 20–1050°C, under a dynamic air atmosphere of 100 μL/min at a heating rate of 10°C/min.

4. Results

4.1. Mechanical Data

In the low P-T stage of the experiment, all samples show a strain hardening behavior, as shear strength increases with axial displacement toward a steady value (Figure 3). In the high P-T stage, red and gray clay samples display a marked strain hardening behavior with axial displacement until the end of the experiment (Figures 3a and 3b). On the other hand, lithological contact samples show an initial strain hardening, which evolves to a steady state or strain weakening in the last ca. 1.5 mm of axial displacement (Figure 3c). From the low to the high P-T

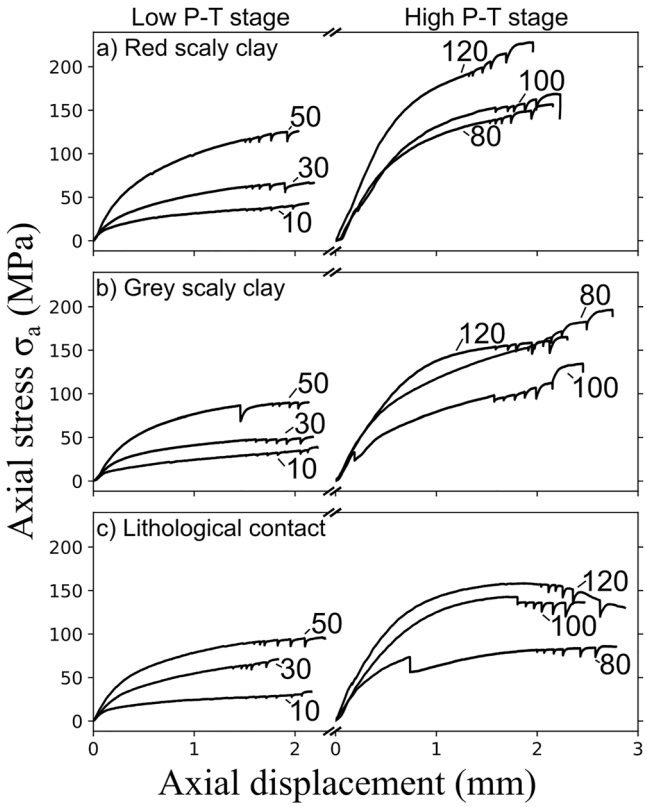

Figure 3. Evolution of axial stress (σ_a) with axial displacement. To effectively overlap the experimental curves, axial displacement was zeroed at the touchpoint value both at the beginning of the low and high P-T stage. The labels on the lines indicate the confining pressure (in MPa) during the test. The experimental curves are presented grouped by material: (a) red clay, (b) gray clay, and (c) red-on-gray clay.

stages, each sample shows a reduction in σ_d/P_c, which suggests a decrease of overall shear strength (Figure 4). Results from the slide-hold-slide tests are not presented because most of the samples did not have a frictional contact (Section 4.2) and therefore frictional healing could not be discussed.

4.2. Microstructures of Starting and Deformed Samples

Polished cross sections of deformed samples cut parallel to the slip direction show a distinctive deformation pattern depending on the sample lithology, clearly distinguishable from that of the starting material (Figure 5). The starting material includes an oblique lithological contact between red and gray clays (Figure 5a). The long axis of scaly clays (S1 foliation, Section 2) are subparallel to the contact. SEM-BSE images show that the microstructures of the gray and red layers both consist of clay lamellae embedding clasts of calcite (<100 μm), illite or mica lamellae and quartz. Calcite clasts are more abundant in the gray layer. Here, two subdomains might be recognized, whose boundary is marked by the presence of calcite vein fragments ("vf," Figure 6a).

Both deformed gray and red clays samples display distributed sigmoidal S-foliation whose angle with the sample boundaries varied from 45°–50° in the axial part of the samples to about 20° toward the boundaries. Distributed contraction is coherent with the observation that in both mono-lithological samples the final offset differs from the left to the right side of the sample, and no through-going offset is observed (see Table S1 in Supporting Information S1, Figures 5b and 5c). The sigmoidal shape of the foliation which tends to become parallel to the contacts with the sample holder suggests that a shear strain was preferentially accommodated along the sample boundaries, coherent with the oblique shape of the sides of the red clay sample in contact with the spacer (Figure 5c).

SEM-BSE images show that the S-foliation is locally highlighted by the alignment of lighter minerals (Figures 6b and 6c). In the red post-mortem

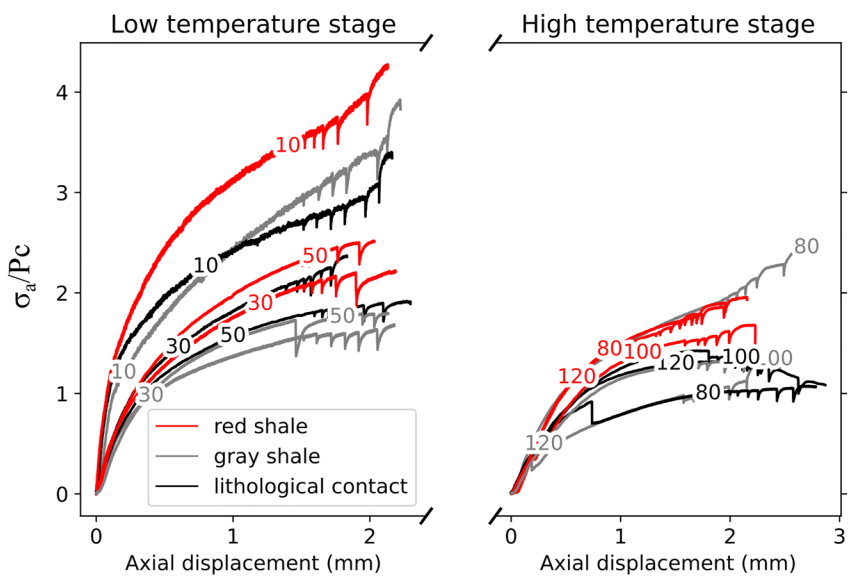

Figure 4. Evolution of the normalized differential axial stress σ_d/P_c with axial displacement. To effectively overlap the experimental curves, axial displacement was zeroed at the touchpoint value both at the beginning of the low and high P-T stage of each experiment. The labels on the lines indicate the confining pressure of the experiment.

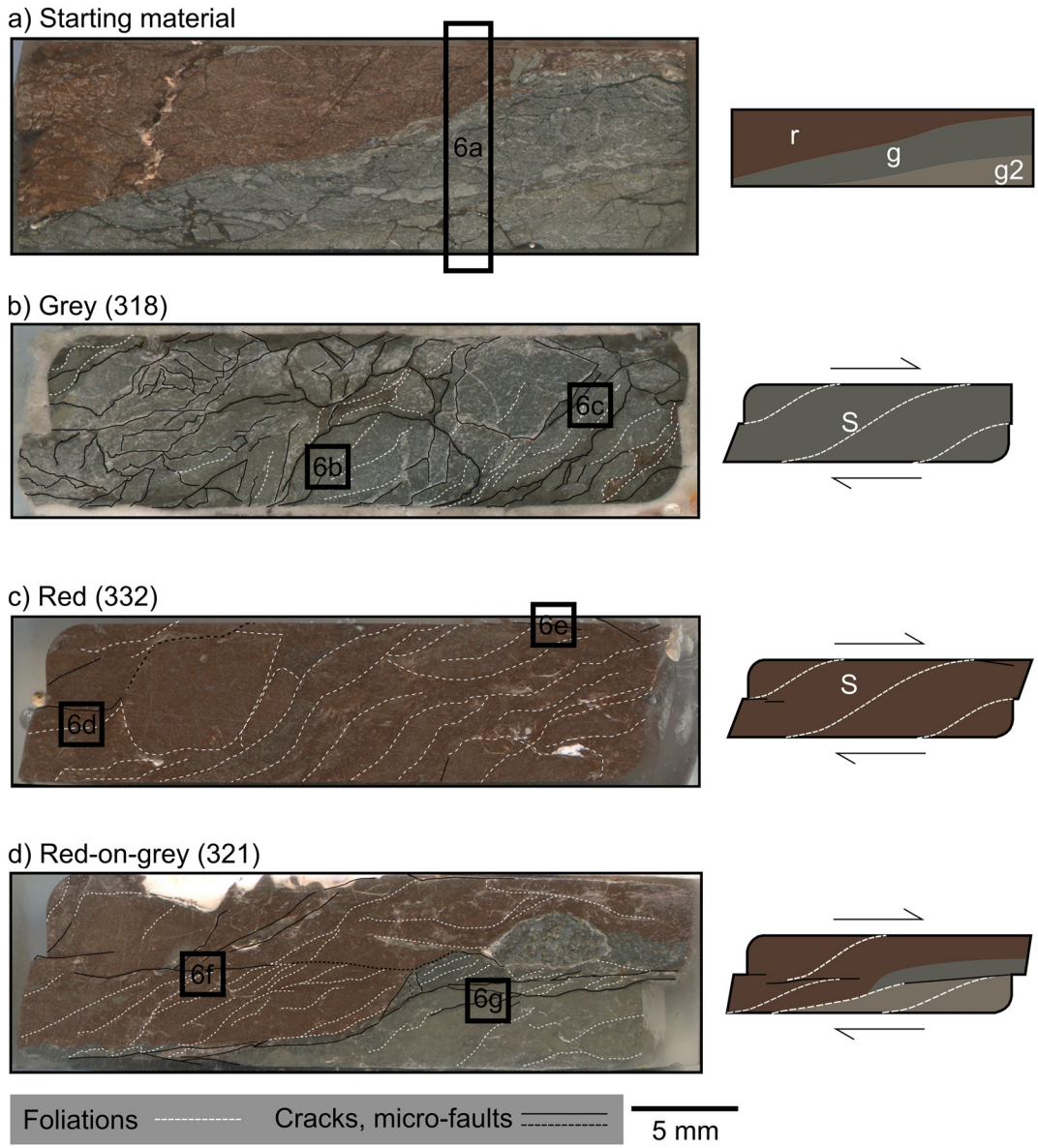

Figure 5. Polished sections of starting and deformed samples cut parallel to the slip direction. The cross sections show interpreted foliations and cracks and small sketches next to each scan interpret the deformation of each sample. Here, light gray lines are the lithological boundary, whereas white or black dashed lines are the foliations and continuous black lines are the cracks or shear surfaces. The sections are: (a) starting red-on-gray material, (b) deformed gray d318, (c) deformed red d332, and (d) deformed red-on-gray d321. Locations of SEM-BSE images of Figure 6 are indicated.

sample, boundary shear results in the formation of shear surfaces at low angle with the boundary. Similar structures are locally visible at the contact between the sample and the piston (Figures 5c, 6d, and 6e).

The deformed red-on-gray sample with the lithological contact have identical offsets on both left and right sides indicating that deformation was more efficiently localized across the sample (Figure 5d). A high-angle sigmoidal S-foliation is deflected both toward the sample boundaries and toward the axial zone. Moving from left to right, low angle shear surfaces, with *en-echelon* pattern, localize shear strain in the axial zone of the sample (Figure 6f), up to when the boundary between two gray domains (g and g2) is reactivated on the right end of the sample (Figure 6g).

The cross section images of the red or gray clay deformed sample (Figure 5d) show that the through going offset is always lower than the total offset imposed during the experiment (Table S1 in Supporting Information S1). In

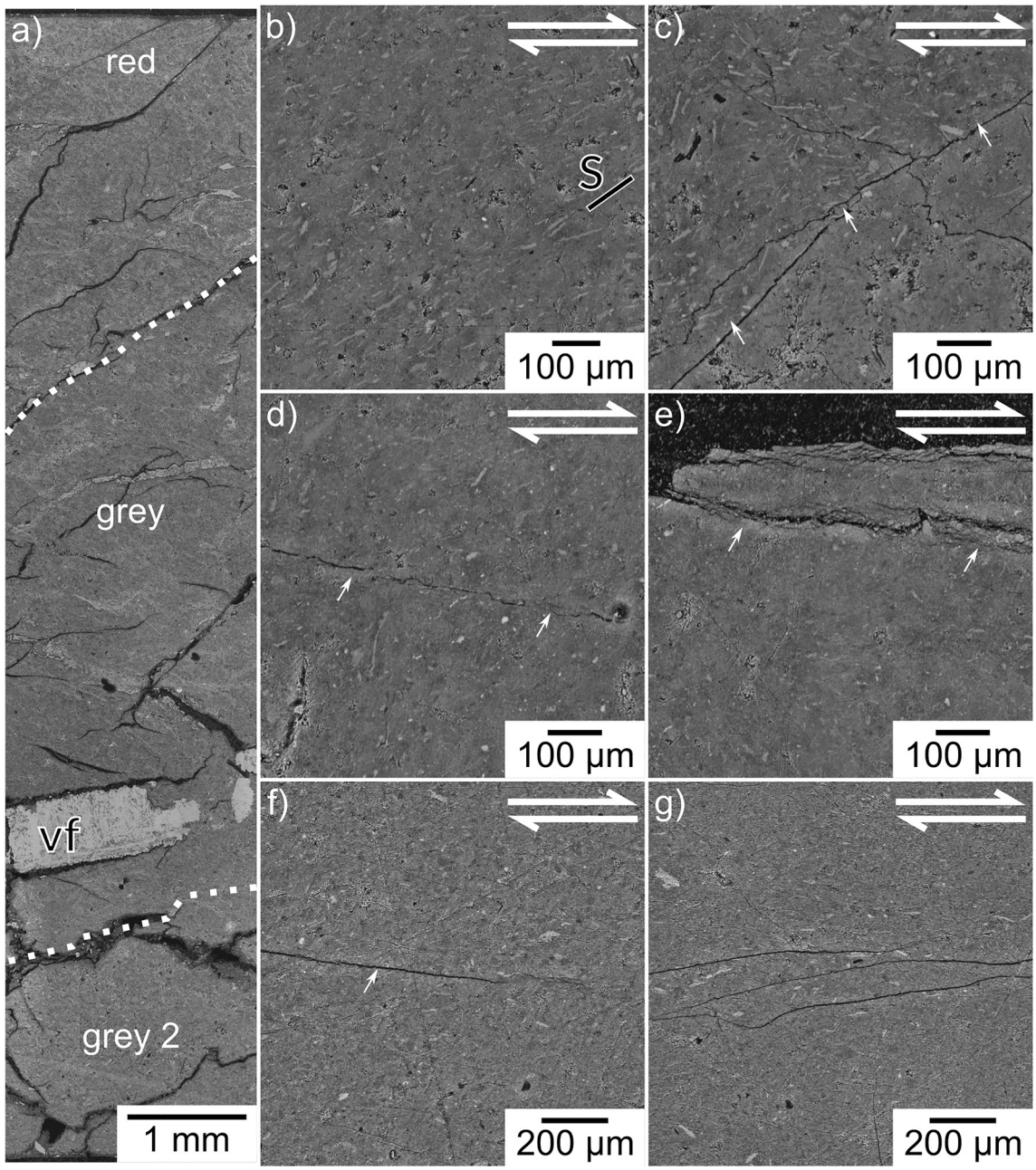

Figure 6. SEM-BSE images of microstructures of the starting and deformed samples shown in Figure 5. (a) Transect across red-on-gray starting material with shown the red-gray and gray-gray 2 domains boundaries, a vein fragment is indicated by "vf"; close-up images from the deformed sample gray d318 foliated domain with (b) continuous S foliation indicated by an oblique marker parallel to major axis of the bright grains and (c) slightly sheared contact between two scaly clays, now slightly open along a shear fracture (black, indicated by white arrows). (d) Close-up images from the deformed sample red d332 with (d) a low-angle shear surface (white arrows), propagating from the offset left edge of the sample and terminating in a series of *én-echelon* cracks after few millimeters into the sample, (e) a low-angle shear surface (white arrows) developing from the top edge of the sample, possibly associated to localization along the contact with the sample holder; close-up images from the deformed sample red-on-gray d321 with (f) a low-angle shear surface (white arrow) developing from the left edge of sample and (g) of the sheared lithological boundary on the left side of the sample.

Figure 5d, the measured offset is very similar to the amount of axial displacement during the last deformation step at constant or decreasing differential stress during the high P-T stage of the experiment (i.e., the last ~1.5 mm of axial displacement). This observation suggest that the deformation is localized effectively only in the last part of the high P-T stage of the experiment, while in the low P-T stages, and at the beginning of the high P-T

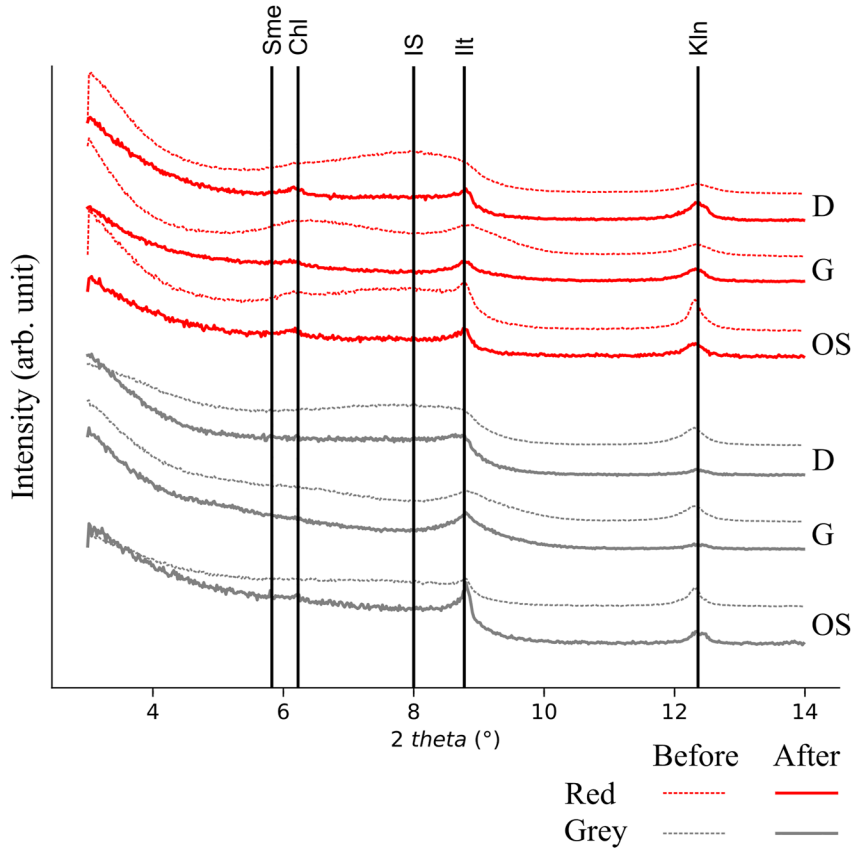

Figure 7. Comparison of X-ray powder diffraction patterns collected on isoriented samples under air dried randomly oriented (D) oriented (OS), and glycolated (G) conditions of the starting (before) and deformed (after) red and gray samples. From left to right theoretical peak positions of Smectite, Chlorite, Illite, and Kaolinite (001) reflections are indicated. The bump centered at ca. 8°2θ indicated the presence of the interstratified illite-smectite (IS).

stages the deformation was likely distributed as suggested also by the formation of a S-foliation similar to that in mono-lithological samples.

4.3. X-Ray Powder Diffraction (XRPD) Analyses

Qualitative observations from XRD analyses on randomly oriented powdered samples indicate that gray and red clays have a very similar mineralogical composition including: illite, kaolinite, interstratified illite-smectite (IS), quartz, calcite, and, limited to the red clay, detectable small amounts of hematite and chlorite. Microstructural observations indicate that calcite is present as small veinlets within the clay (Figure 5). From the diffractogram collected on isoriented samples at low °2θ is possible to observe in both red and gray clays clear variations occurring after the experiments, especially in the region characteristic of IS. The permanent water removal from the interlayer of smectite layers in IS particularly evident comparing diffractograms collected on air dried, oriented, and glycolated samples, where the broad smectite layer 001 peak disappeared and only illite 001 peak remained (Figure 7). Overall, both gray and red clays deformed samples either contain less smectite and less IS with respect to the undeformed samples.

4.4. Thermogravimetric (TG) Analyses

TG analyses measure the weight loss resulting from dehydration reactions triggered by the temperature increase and depend on the minerals present within the tested material. Moreover, since the analyses are performed on both undeformed and deformed samples, the analyses allowed us to compare how our deformation experiments affected the weight loss (Table S2 in Supporting Information S1).

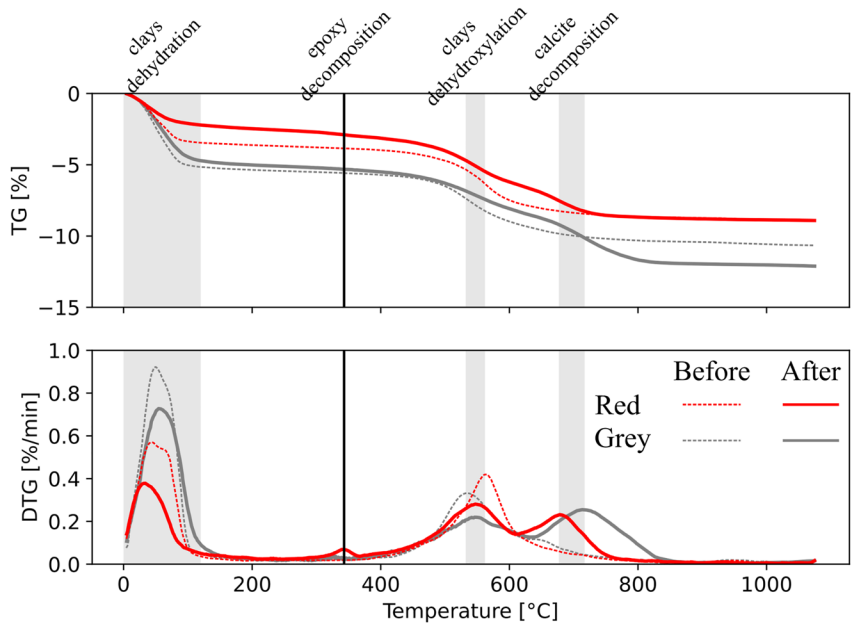

Figure 8. Summary of TG (top panel) and DTG (bottom panel) analyses on randomly oriented samples of the starting (s. m.) and deformed materials. A Savitzky-Golay polynomial filter with window = 51 and polynomial order = 5 was applied to smooth the DTG data. Shaded areas and vertical lines indicate the chemical reactions, from left to right: clays dehydration of pore and interlayer water, epoxy decomposition, clays dehydroxylation, calcite decomposition (decarbonation).

From the evolution of the TG and DTG curves (Figure 8), we recognized four peaks: (a) a broad peak at $0 < T < 150$°C is found in all samples, both deformed and undeformed and is interpreted as due to the dehydration of adsorbed water, both in the pore space and in the smectite interlayers; (b) a peak centered at 532–562°C, common in both gray and red clays, undeformed and deformed, interpreted as the dehydroxylation reaction (i.e., release of OH^- from the mineral lattice); (c) a peak centered at 340°C, interpreted as the thermal decomposition reaction of epoxy resin and therefore considered as contamination and ignored; and (d) a peak centered at 670–715°C, interpreted as the thermal decomposition reaction of carbonates, which are present in both gray and red clays in deformed samples.

From the comparison of the TG and DTG evolution with temperature between starting and deformed materials we observe that both the broad dehydration peak ($0 < T < 150$°C) and the dehydroxylation peak (centered at 532–562°C) are lower in deformed than in undeformed clays (Figure 8). Deformed clays lose less water by dehydration and dehydroxylation reactions and have less smectite (or smectite layers in IS) as observed in XRPD analysis, suggesting that interlayer water was removed permanently from smectite layers in IS during the high P-T stage of the triaxial experiment.

5. Discussion

5.1. Strain Weakening and Localization at High P-T

When sheared in the low P-T stage, red and gray samples show a typical plastic yield followed by strain hardening behavior, regardless of the confining pressure. This behavior is also observed during the high P-T stage of the experiments (Figures 3a and 3b). Conversely, red-on-gray samples containing the lithological contact when deformed at high P-T conditions (Figure 3c) show, after yielding, an evolution toward strain insensitive to weakening behavior. All samples show a significant decrease in the overall value of normalized differential stress between the low and the high P-T stage of the experiment (Figure 4).

Strain weakening or hardening can be associated to microstructural observations of localized or distributed strain in the samples. Distributed strain in an oblique foliation results in increasing work against the confining pressure to thicken the sample and therefore the strain hardening behavior. This interpretation is supported by the diffuse S-foliation registered in samples of gray and red clays that displayed only strain hardening behavior (Figures 5b,

Table 1
Factors Influencing Shear Localization Inferred From Laboratory Experiments Applied to a Natural Accretionary Prism

Our experiments	Accretionary prism
Lithological contact	Contrast in viscosity and elastic properties promoting stress concentration
High P-T stage: P_c > 100 MPa and T = 150°C	Availability of water in areas with lower stress concentration (temperature, wt.% of smectite, degree of compaction)
Closed system (undrained conditions)	Low permeability of host rocks

5c, 5e, and 5f). On the other hand, strain weakening observed in samples with the lithological contact is associated with strain localization along low angle and boundary shear surfaces. Localization in samples with a lithological contact is highlighted by the presence of offset on both sides of the sample assembly (Figures 5a and 5d). The offset coincides with the amount of axial displacement during the steady state or strain weakening stage of the experiments at high P-T (ca. 1.5 mm). Shear surfaces in the red-on-gray sample link the two opposite sides of the sample allowing for the observed offset.

Our observations show that strain localization occurs just where a lithological boundary is present, and when the highest temperatures (150°C) and confining stresses (120 MPa) are achieved. This temperature likely affect the rheology of the samples also changing permanently the lattice structure of the clays due to the interlayer dehydration of smectite clays (Schleicher et al., 2015). For the composition of our samples, these temperatures coincide with a 10 to 12 or 9 wt.% cumulative weight loss in gray or red clays (Table S2 in Supporting Information S1). Notably, both gray and red clays showed, after deformation, a reduction in smectite content from the interlayered smectite-illite, which is likely related to the collapse of the smectite interlayer starting at 90°C (Ferrage et al., 2007). Transformation of smectite into illite, which occurs at temperatures of about 150°C, did not likely occur in our experiments. In fact, transformation of smectite into illite was likely hindered by the unavailability of K+ ions and insufficient time for the reaction (Cuadros & Linares, 1996).

Water release by dehydration might pressurise and reduce the effective normal stress on shear surfaces across our samples and can act as a lubricant in clay interlayers (Aretusini et al., 2019; Ferri et al., 2011; King Hubbert & Rubey, 1959). Therefore, dehydration contributed to the lower σ_d/P_c observed during the high P-T stage of all experiments with respect to their low P-T stage (Figure 4). Fluid pressurisation is favoured by undrained conditions imposed during the experiments and by the low permeability of our clays (D. E. Moore & Lockner, 2007; Morrow et al., 2017). Given the high content of clays and low permeability of smectite, generally in the range from $\sim 10^{-21}$ to 10^{-23} m^2 (Behnsen & Faulkner, 2013), undrained conditions can be reasonably assumed also when smectite-rich rocks are deformed within the accretionary prism. Our data suggests that water release occurs in all samples, but weakening occurs just in presence of a lithological contact. In this case, the strain weakening behavior might have been enhanced by the slight permeability and viscosity contrast of the two clays. It is worth noting that grey is often weaker than red scaly clays at same P_c (Figure 4), even if the composition of the two clays is indistinguishable by mineralogical analysis. When juxtaposed across the contact, a small viscosity contrast and/or a small difference in permeability between the two clays, may cause a local strain rate gradient. Moreover, the viscosity contrast may induce a local "underpressure" close and/or along the interface, enhanced by the wavy geometry of the contact (Mancktelow, 2008). As a consequence, a local pressure drop might focus fluid flow facilitating shear along the lithological contact. In this perspective, the occurrence of the lithological contact is probably a necessary but not sufficient feature to promote strain weakening, as both strain localization and water release by dehydration reactions are concurrent in controlling strain weakening.

5.2. Implications for the Mechanical Behavior of Clay-Rich Sediments in Subduction Zones

Deformation of clays at shallow depth is associated with the pervasive development of a scaly fabric, which is classically interpreted as an evidence for de-localization of deformation (J. C. Moore, 1986). This would indicate a strain hardening mechanical behavior. On the other hand, in the same geological settings, sharp, localized shear zones are observed at all scales (Vannucchi, 2019), therefore suggesting that under certain conditions strain localization is favored. While strain localization is an indication for (strain) slip weakening mechanical behavior and might potentially be associated with unstable slip, the factors that control its occurrence are yet poorly understood. Alternatively, the scaly fabric might also be an expression of a bulk de-localized strain hardening deformation by means of highly strain-localized but intermittently active and anastomosing slip zones (Tarling & Rowe, 2016). Localization versus de-localization of strain in scaly clays is therefore crucial to shed light on what promotes alternation between hardening and weakening processes in these rocks that might influence their mechanical behavior (Table 1).

Contemporary subduction zones are characterized by sediments accumulating in the accretionary prisms, which are poorly lithified, and have larger water content and porosity with respect to the scaly clays tested here. These sediments undergo load strengthening stress paths during burial, and during deformation within the accretionary prism the porosity decreases dramatically (Bray & Karig, 1985). Their mechanical behavior depends on the initial porosity and consolidation state: with the same applied stress path, strongly

over-consolidated sediments fail in a brittle way, whereas normal-consolidated sediments fail in a ductile way (Karig & Morgan, 1994). Such behaviors have been well described by the concept of critical state soil mechanics (Wood, 1990), which does not require high temperature to facilitate strain localization and promote brittle behavior (Morgan et al., 2022). Within the Ligurian accretionary complex, the red and gray scaly clays tested in this study belonged to the same fossil accretionary prism, and therefore had a similar burial, polyphasic folding deformation, late brittle deformation and exhumation history. During this complex history, the scaly clay fabric developed during ductile yielding in the folding stage, likely under a normal-consolidated state, similar to contemporary sediments after they entered the accretionary prism and started being accreted in the proto-thrust zone and then behind the frontal thrust (Karig & Morgan, 1994). Then, after the folding event leading to the formation of scaly clays, the sediments underwent consolidation before being exhumed. All the three types of scaly clays tested in our experiments (red, gray, and red-on-gray) showed a clear strain hardening behavior at low confining pressures (10, 30, and 50 MPa) and room temperature indicative of ductile failure and post-failure strain hardening (low P-T stage in Figures 3 and 4). At higher confining pressures (80, 100, and 120 MPa) and 150°C, gray and red still display ductile failure and post-failure strain hardening (high P-T stage in Figures 3 and 4). On the other hand, red-on-gray show a progressive evolution from strain neutral to strain weakening with increasing confining pressure, compatible with ductile failure evolving to brittle failure and strain localization. This behavior indicative of brittle failure at the highest confining pressures might be compatible with the pore fluid pressure increase due to pressurization of the released water in pores due to the dehydration of smectite layers in interlayered IS promoted by the undrained conditions of the experiment, possibly combined with the smallest porosity achieved in the sample when deformed at the highest confining pressures.

Our experiments were therefore performed on over-consolidated clays which are under a different consolidation state with respect to the pelagic clays undergoing deformation within the nowadays accretionary prisms. However, we suggest that high temperatures and associated fluid release alone are insufficient to induce localization and brittle behavior. Even with small compositional and microstructural differences, lithological contrasts, either inherited by the sedimentation or shaped by diffuse deformation at shallow burial conditions, are critical to promote localization and brittle behavior. This is indeed coherent with the field observations of enhanced strain localization at the contact juxtaposing different clays within the fossil accretionary of the Argille Varicolori in the Northern Apennines. Here, strain localization at the lithological boundaries, at the time of formation might result in rheological contrast of viscosity or yield strength depending on water content, porosity, and mineral composition.

6. Conclusions

We deformed rocks preserving their scaly clay fabric: gray and red clays and one red-on-gray sample encompassing a lithological contact, all sampled from an exhumed accretionary prism. The samples were deformed in a triaxial apparatus, in two subsequent stages: a low P-T stage (i.e., at 22°C with confining pressure of 10, 30, and 50 MPa) and a high P-T stage (i.e., at 150°C, with confining pressure of 80, 100, and 120 MPa). All samples show strain hardening behavior and diffuse deformation at low P-T deformation. During the high P-T stage, all samples show a bulk weakening with respect to the low P-T stage, measured as the axial stress normalized by the confining pressure. During this stage clay samples maintain their ductile behavior whereas the samples containing a lithological contact evolve into strain weakening shearing. Also, deformed samples containing a lithological contact are the only to show through-going offsets consistent with strain localization during the last 1.5 mm of axial displacement. After the high P-T stage, red or gray clays display a lower water content and lower smectite layers in the IS interlayers, with respect to their original state. This indicates, together with the bulk weakening, that water is released from smectite due to dehydration under undrained conditions. Collectively, our experiment indicate that lithological contacts may favor strain localization, strain weakening and brittle behavior when deformed at in situ P-T conditions typical of burial in the accretionary wedge, even when the difference in the mineral composition and internal textures are apparently negligible.

Data Availability Statement

The mechanical data presented here (Section 4.1) are available at (Aretusini & Tesei, 2022).

Acknowledgments
This work was supported by the European Commission through the Marie Sklodowska-Curie Fellowship STRAIN (748400) to TT. SA participated in this work in the framework of the European Research Council (ERC) project FEAR (Grant 856559) under the European Community's Horizon 2020 Framework Programme. The authors acknowledge two anonymous reviewers whose comments greatly improved the manuscript.

References

Aretusini, S., Spagnuolo, E., Dalconi, M. C., Di Toro, G., & Rutter, E. H. (2019). Water availability and deformation processes in smectite-rich gouges during seismic slip. *Journal of Geophysical Research: Solid Earth*, *124*(11), 10855–10876. https://doi.org/10.1029/2019JB018229

Aretusini, S., & Tesei, T. (2022). Direct shear (triaxial apparatus) data for the manuscript: "Heterogeneity-driven localisation and weakening in scaly clays from a fossil accretionary prism." (version 1.0) [Dataset]. Zenodo. https://doi.org/10.5281/zenodo.7274387

Behnsen, J., & Faulkner, D. R. (2013). Permeability and frictional strength of cation-exchanged montmorillonite. *Journal of Geophysical Research: Solid Earth*, *118*(6), 2788–2798. https://doi.org/10.1002/jgrb.50226

Bettelli, G., & De Nardo, M. T. (2001). Geological outlines of the Emilia Apennines (Italy) and introduction to the rock units cropping out in the areas of the landslides reactivated in the 1994–1999 period. *Quaderni di Geofisica Applicata*, *8*(1), 1–26.

Bettelli, G., & Vannucchi, P. (2003). Structural stlyle of the offscraped Ligurian oceanic sequences of the Northern Apennines: New hypothesis concerning the development concerning the development of meélange block-in-matrix fabric. *Journal of Structural Geology*, *25*(3), 371–388. https://doi.org/10.1016/S0191-8141(02)00026-3

Bray, C. J., & Karig, D. E. (1985). Porosity of sediments in accretionary prisms and some implications for dewatering processes. *Journal of Geophysical Research*, *90*(B1), 768–778. https://doi.org/10.1029/JB090iB01p00768

Byrne, T., & Fisher, D. (1990). Evidence for a weak and overpressured décollement beneath sediment-dominated accretionary prisms. *Journal of Geophysical Research*, *95*(B6), 9081–9097. https://doi.org/10.1029/JB095IB06P09081

Collettini, C., Niemeijer, A. R., Viti, C., & Marone, C. (2009). Fault zone fabric and fault weakness. *Nature*, *462*(7275), 907–910. https://doi.org/10.1038/nature08585

Cowan, D. S., & Silling, R. M. (1978). A dynamic, scaled model of accretion at trenches and its implications for the tectonic evolution of subduction complexes. *Journal of Geophysical Research*, *83*(B11), 5389–5396. https://doi.org/10.1029/JB083IB11P05389

Cuadros, J., & Linares, J. (1996). Experimental kinetic study of the smectite-to-illite transformation. *Geochimica et Cosmochimica Acta*, *60*(3), 439–453. https://doi.org/10.1016/0016-7037(95)00407-6

Ferrage, E., Kirk, C. A., Cressey, G., & Cuadros, J. (2007). Dehydration of Ca-montmorillonite at the crystal scale. Part 2. Mechanisms and kinetics. *American Mineralogist*, *92*(7), 1007–1017. https://doi.org/10.2138/am.2007.2397

Ferri, F., Di Toro, G., Hirose, T., Han, R., Noda, H., Shimamoto, T., et al. (2011). Low-to high-velocity frictional properties of the clay-rich gouges from the slipping zone of the 1963 Vaiont Slide, Northern Italy. *Journal of Geophysical Research*, *116*(B9), 1–17. https://doi.org/10.1029/2011JB008338

Festa, A., Pini, G. A., Dilek, Y., Codegone, G., Vezzani, L., Ghisetti, F., et al. (2009). Peri-Adriatic mélanges and their evolution in the Tethyan realm (Vol. *52*, pp. 369–403). https://doi.org/10.1080/00206810902949886

Harbord, C. W. A., Nielsen, S., Paola, N. D., & Holdsworth, R. E. (2017). Earthquake nucleation on rough faults. *Geology*, *45*(10), 931–934. https://doi.org/10.1130/G39181.1

Hilde, T. W. C. (1983). Sediment subduction versus accretion around the pacific. *Tectonophysics*, *99*(2–4), 381–397. https://doi.org/10.1016/0040-1951(83)90114-2

Ikari, M. J., Ito, Y., Ujiie, K., & Kopf, A. J. (2015). Spectrum of slip behaviour in Tohoku fault zone samples at plate tectonic slip rates. *Nature Geoscience*, *8*(11), 870–874. https://doi.org/10.1038/ngeo2547

Karig, D., & Morgan, J. (1994). Tectonic deformation: stress paths and strain histories. In Alex Maltman (Ed.), *The geological deformation of sediments* (pp. 167–204). Springer Netherlands. https://doi.org/10.1007/978-94-011-0731-0_6

King Hubbert, M., & Rubey, W. W. (1959). Role of fluid pressure in mechanics of overthrust faulting: I. Mechanics of fluid-filled porous solids and its application to overthrust faulting. *GSA Bulletin*, *70*(2), 115–166. https://doi.org/10.1130/0016-7606(1959)70[115:ROFPIM]2.0.CO;2

Kirkpatrick, J. D., Rowe, C. D., Ujiie, K., Moore, J. C., Regalla, C., Remitti, F., et al. (2015). Structure and lithology of the Japan Trench subduction plate boundary fault. *Tectonics*, *34*(1), 53–69. https://doi.org/10.1002/2014TC003695

Kubo, T., & Katayama, I. (2015). Effect of temperature on the frictional behavior of smectite and illite. *Journal of Mineralogical and Petrological Sciences*, *110*(6), 293–299. https://doi.org/10.2465/jmps.150421

Labaume, P., Maltman, A., Bolton, A., Tessier, D., Ogawa, Y., & Takizawa, S. (1997). Scaly fabrics in sheared clays from the décollement zone of the Barbados accretionary prism. *Proceedings of the Ocean Drilling Program, Scientific Results*, *156*, 59–77.

Maltman, A., & Vannucchi, P. (2004). Insights from the Ocean Drilling Program on shear and fluid-flow at the mega-faults between actively converging plates. *Geological Society, London, Special Publications*, *224*(1), 127–140. https://doi.org/10.1144/GSL.SP.2004.224.01.09

Mancktelow, N. S. (2008). Tectonic pressure: Theoretical concepts and modelled examples. *Lithos*, *103*(1–2), 149–177. https://doi.org/10.1016/j.lithos.2007.09.013

Moore, D. E., & Lockner, D. A. (2007). Friction of the smectite clay montmorillonite. *The seismogenic zone of subduction thrust faults*, (pp. 317–345).

Moore, J. C. (1986). *Structural fabric in Deep Sea Drilling Project cores from forearcs* (Vol. 166). Geological Society of America.

Moore, J. C., Plank, T. A., Chester, F. M., Polissar, P. J., & Savage, H. M. (2015). Sediment provenance and controls on slip propagation: Lessons learned from the 2011 Tohoku and other great earthquakes of the subducting northwest Pacific plate. *Geosphere*, *11*(3), 533–541. https://doi.org/10.1130/GES01099.1

Moore, J. C., & Saffer, D. M. (2001). Updip limit of the seismogenic zone beneath the accretionary prism of Southwest Japan: An effect of diagenetic to low-grade metamorphic processes and increasing effective stress. *Geology*, *29*(2), 183. https://doi.org/10.1130/0091-7613(2001)029<0183:ULOTSZ>2.0.CO;2

Morgan, J. K., Solomon, E. A., Fagereng, A., Savage, H. M., Wang, M., Meneghini, F., et al. (2022). Seafloor overthrusting causes ductile fault deformation and fault sealing along the Northern Hikurangi Margin. *Earth and Planetary Science Letters*, *593*, 117651. https://doi.org/10.1016/j.epsl.2022.117651

Morrow, C. A., Moore, D. E., & Lockner, D. A. (2017). Frictional strength of wet and dry montmorillonite. *Journal of Geophysical Research: Solid Earth*, *122*(5), 3392–3409. https://doi.org/10.1002/2016jb013658

Oleskevich, D. A., Hyndman, R. D., & Wang, K. (1999). The updip and downdip limits to great subduction earthquakes: Thermal and structural models of Cascadia, south Alaska, SW Japan, and Chile. *Journal of Geophysical Research*, *104*(B7), 14965–14991. https://doi.org/10.1029/1999JB900060

Pini, G. A. (1999). Tectonosomes and olistostromes in the Argille Scagliose of the Northern Apennines, Italy. https://doi.org/10.1130/SPE335

Remitti, F., Balestrieri, M. L., Vannucchi, P., & Bettelli, G. (2013). Early exhumation of underthrust units near the toe of an ancient erosive subduction zone: A case study from the Northern Apennines of Italy. *GSA Bulletin*, *125*(11–12), 1820–1832. https://doi.org/10.1130/B30862.1

Remitti, F., Bettelli, G., Panini, F., Carlini, M., & Vannucchi, P. (2012). Deformation, fluid flow, and mass transfer in the forearc of convergent margins: A two-day field trip in an ancient and exhumed erosive convergent margin in the Northern Apennines. *GSA Field Guides*, *28*, 1–33. https://doi.org/10.1130/2012.0028(01)

Saffer, D. M., & Tobin, H. J. (2011). Hydrogeology and mechanics of subduction zone forearcs: Fluid flow and pore pressure (Vol. *39*, pp. 157–186). https://doi.org/10.1146/ANNUREV-EARTH-040610-133408

Sawai, M., Hirose, T., & Kameda, J. (2014). Frictional properties of incoming pelagic sediments at the Japan trench: Implications for large slip at a shallow plate boundary during the 2011 Tohoku earthquake. *Earth Planets and Space*, *66*(1), 1–8. https://doi.org/10.1186/1880-5981-66-65

Schleicher, A. M., Boles, A., & van der Pluijm, B. A. (2015). Response of natural smectite to seismogenic heating and potential implications for the 2011 Tohoku earthquake in the Japan trench. *Geology*, *43*(9), 755–758. https://doi.org/10.1130/G36846.1

Schleicher, A. M., van der Pluijm, B. A., & Warr, L. N. (2010). Nanocoatings of clay and creep of the San Andreas fault at Parkfield, California. *Geology*, *38*(7), 667–670. https://doi.org/10.1130/G31091.1

Tarling, M. S., & Rowe, C. D. (2016). Experimental slip distribution in lentils as an analog for scaly clay fabrics. *Geology*, *44*(3), 183–186. https://doi.org/10.1130/G37306.1

Tesei, T., Collettini, C., Barchi, M. R., Carpenter, B. M., & Di Stefano, G. (2014). Heterogeneous strength and fault zone complexity of carbonate-bearing thrusts with possible implications for seismicity. *Earth and Planetary Science Letters*, *408*, 307–318. https://doi.org/10.1016/J.EPSL.2014.10.021

Tesei, T., Lacroix, B., & Collettini, C. (2015). Fault strength in thin-skinned tectonic wedges across the smectite-illite Transition: Constraints from friction experiments and critical Tapers. *Geology*, *43*(10), 923–926. https://doi.org/10.1130/G36978.1

Thomson, S. N., Brandon, M. T., Reiners, P. W., Zattin, M., Isaacson, P. J., & Balestrieri, M. L. (2010). Thermochronologic evidence for orogen-parallel variability in wedge kinematics during extending convergent orogenesis of the northern Apennines, Italy. *GSA Bulletin*, *122*(7–8), 1160–1179. https://doi.org/10.1130/B26573.1

Vannucchi, P. (2019). Scaly fabric and slip within fault zones. *Geosphere*, *15*(2), 342–356. https://doi.org/10.1130/GES01651.1

Vannucchi, P., & Bettelli, G. (2002). Mechanisms of subduction accretion as implied from the broken formations in the Apennines, Italy. *Geology*, *30*(9), 835. https://doi.org/10.1130/0091-7613(2002)030<0835:MOSAAI>2.0.CO;2

Vannucchi, P., Maltman, A., Bettelli, G., & Clennell, B. (2003). On the nature of scaly fabric and scaly clay. *Journal of Structural Geology*, *25*(5), 673–688. https://doi.org/10.1016/S0191-8141(02)00066-4

Vannucchi, P., Remitti, F., & Bettelli, G. (2008). Geological record of fluid flow and seismogenesis along an erosive subducting plate boundary. *Nature*, *451*(7179), 699–703. https://doi.org/10.1038/nature06486

Vrolijk, P. (1990). On the mechanical role of smectite in subduction zones. *Geology*, *18*(8), 703–707. https://doi.org/10.1130/0091-7613(1990)018<0703:OTMROS>2.3.CO;2

Wood, D. M. (1990). *Soil behaviour and critical state soil mechanics*. Cambridge University Press.